TRASONIC IMAGING 10, 81-89

DEVIATIONS FROM RAYLEIGH STATISTICS IN ULTRASONIC SPECKLE

T.A. Tuthill, R.H. Sperry and K.J. Parker

University of Rochester
Rochester, NY 14627

The statistics of speckle patterns in ultrasound images have potential for tissue characterization. In "fully developed speckle" from many random scatterers, the amplitude is widely recognized as possessing a Rayleigh distribution. This study examines how scattering populations and signal processing can produce non-Rayleigh distributions. The first order speckle statistics are shown to depend on random scatterer density and the amplitude and spacing of added periodic scatterers. Envelope detection, amplifier compression, and signal bandwidth are also shown to cause distinct changes in the signal distribution.

Key words: Rayleigh statistics; scatterer populations; simulations; speckle; system effects; tissue characterization.

I. INTRODUCTION

The propagation of ultrasound in parenchymal tissue is fundamentally a statistical process, and numerous tissue characterization techniques are based on this concept. Both the radio-frequency (RF) and envelope signals of backscattered echoes can be analyzed using standard stochastic signal theory. In B-scans of liver parenchyma, the image texture has been compared to laser speckle [1,2] and associated with the same statistical properties. For completely random scatterers, the fully developed speckle patterns are characterized by a Rayleigh distribution [3], in which only the mean backscatter amplitude provides information, as the second order statistics are governed by the system's resolution. The speckle also reduces lesion contrast detection and, consequently, has sometimes been minimized by compounding [4] or filtering [5]. Yet, the liver stroma is comprised of lobules constructed about central veins and bordered by portal triads [6]; thus, "structure" has been suggested as a cause of non-Rayleigh statistics. First order statistics, such as the signal-to-noise ratio (SNR), have been used as discriminators in liver [7] and cardiac [8,9] studies. Assuming the presence of periodic scatterers, the mean spacing can be estimated from the autocorrelation of the RF power spectrum [10-12]. Wagner, Smith, Insana, and colleagues [13-17] employ second order statistics with theory developed from Rician distributions for lesion detection. Another study [18] looked at fourth order moments to obtain a tissue signature.

This report is concerned only with first order statistics in an attempt to better understand the physical causes for the various observed statistical parameters. It begins with simple acoustic models for generating Rayleigh and non-Rayleigh distributions, and demonstrates artifacts which can result from signal processing. Simulations, theory, and clinical data are used to illustrate the influence of scatterer populations and system effects on first order statistics.

0161-7346/88 $3.00

II. THEORY

The derivations for Rayleigh and Rician distributions are given in Middleton [19] and outlined below. For multiple random reflections in a sample volume, the received echo is a random signal

$$s(t) = x(t)\cos(\omega_0 t) - y(t)\sin(\omega_0 t) \tag{1}$$

where ω_0 is the center frequency, and the quadrature components x(t) and y(t) are independent and zero-mean Gaussian. The calculated envelope r(t) may be expressed by the quadrature components

$$r(t) = \sqrt{x^2(t) + y^2(t)} \tag{2}$$

or by a sum using the Hilbert transform $\hat{s}(t)$

$$r(t) = | s(t) + j\hat{s}(t) | \ . \tag{3}$$

The envelope then has a Rayleigh probability density function $p_r(r)$,

$$p_r(r) = \frac{r}{\sigma^2} e^{-r^2/2\sigma^2} \tag{4}$$

where σ^2 is the variance of the quadrature components, and the signal-to-noise ratio is a constant,

$$SNR = \frac{<r>}{\sigma} = 1.91 \ . \tag{5}$$

For the case of few scatterers per sample volume, the speckle is not fully developed and has a lower (<1.9) SNR. The distribution is then termed pre-Rayleigh.

If an additional signal (due possibly to "structure" or periodic scatterers),

$$s'(t) = A(t)\cos(\omega_0 t + \Theta(t)) \tag{6}$$

is combined with a Rayleigh RF signal, the revised distribution has the form

$$p_r(r) = \frac{r}{\sigma^2} e^{-[r^2 + A^2(t)]/2\sigma^2} I_0\left[\frac{A(t)r}{\sigma^2}\right] \tag{7}$$

where $I_0(\ )$ is the modified Bessel function. If A(t) is constant, the distribution is labeled Rician, a term used in optics to describe laser speckle in the presence of a coherent background with constant intensity [3].

III. EFFECTS OF SCATTERER POPULATIONS

For this study, a simple 1-dimensional model was employed using a Gaussian-enveloped pulse with center frequency 2.5 MHz and a -6dB bandwidth of 0.94 MHz. In the time domain, the Gaussian standard deviation, σ, equals 0.4 μs, and we define the pulse width, ΔT, as 4σ (1.6 μs). The sampling rate was 30 MHz. Scatterers were modeled by discrete reflectors of random height (from -1 to 1) and spacing (both with uniform distributions, though other distributions were also studied). The RF signal was derived by convolving the pulse with a scattering train to form a 2000 point waveform analagous to 5 cm of tissue. Each analysis used ten independent lines, corresponding to a large region of interest in a tissue scan. The envelopes were calculated using the Hilbert transform in the frequency domain, and histograms were computed from the ten scan lines.

a) Random Scatterers

The initial study looked at the effects of scatterer density as described by the number of scatterers per pulse width, ranging from sparse to densely packed. The sparse reflector densities give pre-Rayleigh distributions with low SNRs, a result previously noted by Oosterveld [20]. Figure 1a shows a scan line for 2 scatterers/ΔT, along with its analytic envelope. In this and subsequent examples, a histogram curve fit is obtained from the maximum likelihood estimate for a Rayleigh distribution [21], $\sigma^2 = (\Sigma r^2)/2N$, where N is the number of samples. In figure 1b, the curve fit (dotted line) is shown to deviate from the envelope histogram. As the density increases, the histograms approach Rayleigh distributions. For five or more scatterers/ΔT (a typical scan line is shown in figure 2a), the SNR remains at 1.9±0.1 (Fig. 2b).

b) Bimodal Populations

A possibly more realistic modeling of liver parenchyma involves bimodal distributions, formed by adding different classes of scatterers to the densely packed case. The effects of amplitude, spacing, and periodicity were examined for both resolvable (spacings greater than 2λ) and subresolvable strong scatterers superimposed on a train of dense random scatterers which by themselves would generate Rayleigh statistics. In each of the following simulations, the periodic scatterers had an amplitude four times the mean amplitude of the random scatterers.

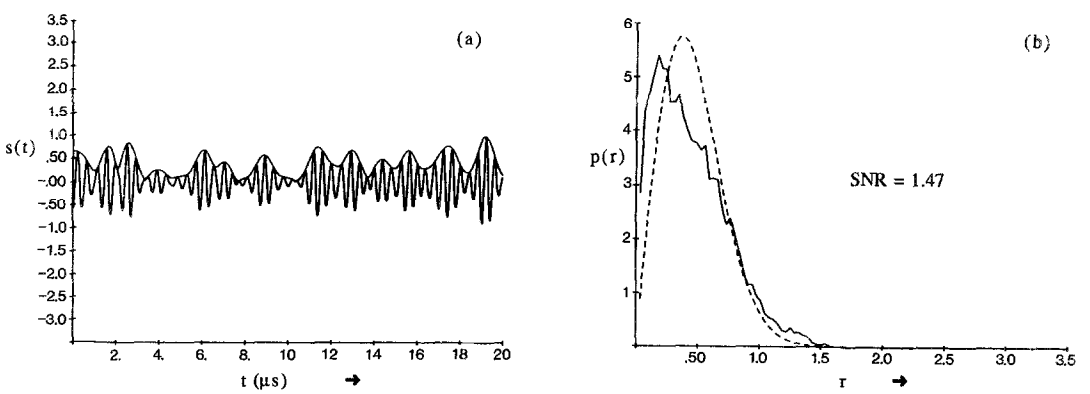

Fig. 1 a) Simulated RF signal for sparse scatterers (2 scatterers/ΔT) and analytic envelope. b) Corresponding envelope histogram with Rayleigh curve fit (dotted line).

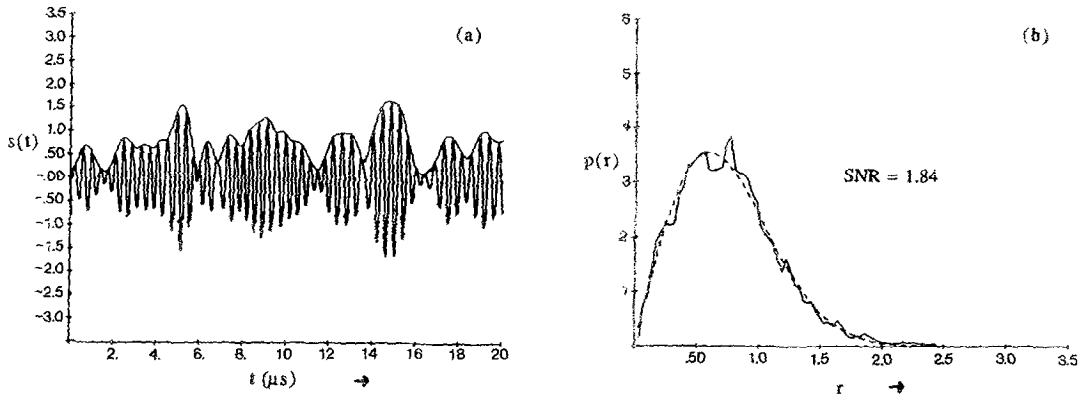

Fig. 2 a) Simulated RF signal for dense scatterers (5 scatterers/ΔT) and analytic envelope. b) Corresponding envelope histogram with Rayleigh curve fit (dotted line).

For strong, sparse scatterers, simulating occasional small arteries in tissue, the envelope distribution appears pre-Rayleigh (Fig. 3), and the SNR drops below 1.9. This addition of occasional strong scatterers causes a wider variation in amplitudes and an increase in σ that is larger than the increase in <r>; thus the SNR decreases. In contrast, for strong, periodic, just-resolvable (~2λ spacing) scatterers, the histogram (Fig. 4), is shifted to a Rician-like distribution with a high SNR.

However, as the spacing of the strong periodic scatterers is decreased to the extent where they become subresolvable, the distributions are highly dependent on the ratio of the periodic scatterer spacing to the wavelength. This concept is similar to the Bragg condition in X-ray diffraction. With spacings close to an integral number of wavelengths, returning echoes interfere constructively, providing a dominant signal. Here again, the SNR is

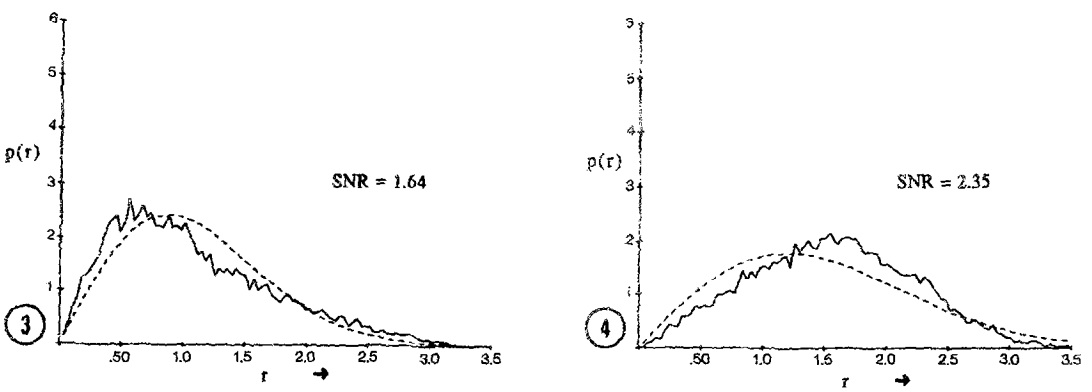

Fig. 3 Envelope histogram for bimodal scatterer distribution of strong, sparse scatterers with dense random scatterers (dotted line is Rayleigh curve fit).

Fig. 4 Envelope histogram for bimodal scatterer distribution of strong, periodic, just resolvable scatterers with dense random scatterers (dotted line is Rayleigh curve fit).

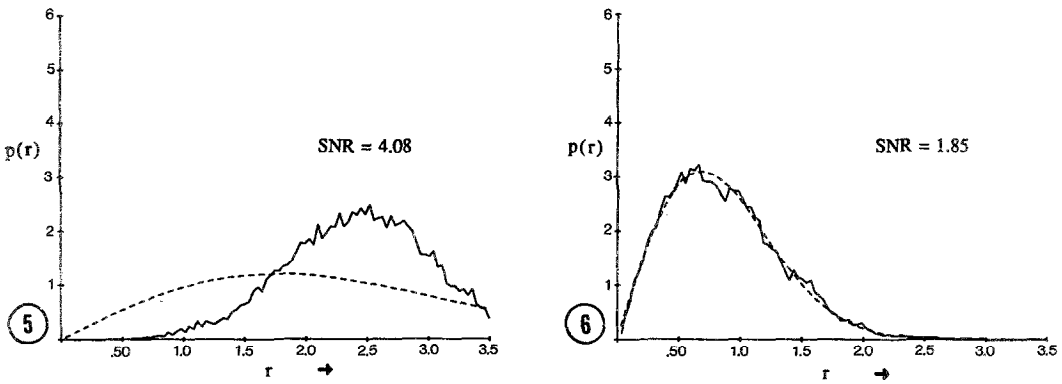

Fig. 5 Envelope histogram for bimodal scatterer distribution of dense random scatterers and strong, periodic, subresolvable scatterers with integral wavelength spacing (dotted line is Rayleigh curve fit).

Fig. 6 Envelope histogram for bimodal scatterer distribution of dense random scatterers and strong, periodic, subresolvable scatterers with spacing of an odd number of half-wavelengths (dotted line is Rayleigh curve fit).

greater than 1.9, and the distribution is Rician-like (Fig. 5). As the scatterer spacing approaches an odd number of half-wavelengths, the SNR drops to 1.9 (Fig. 6). In this case, destructive interference cancels out any effect of the added periodic scatterers, and the distribution is reduced to Rayleigh.

Figure 7 summarizes the equivocal relationship between periodic scatterer spacing and SNR as suggested by Wagner's theoretical analysis [17]. Note the large variation in SNRs for the subresolvable cases. For spacings greater than a pulsewidth, the SNR remains below 1.9. The addition of 10 percent amplitude and spacing jitter to the periodic scatterers decreases the SNR towards the Rayleigh 1.9 for small spacings while maintaining a low SNR for large spacings (dashed line). A reduction in the amplitude of the periodic scatterers has a similar effect.

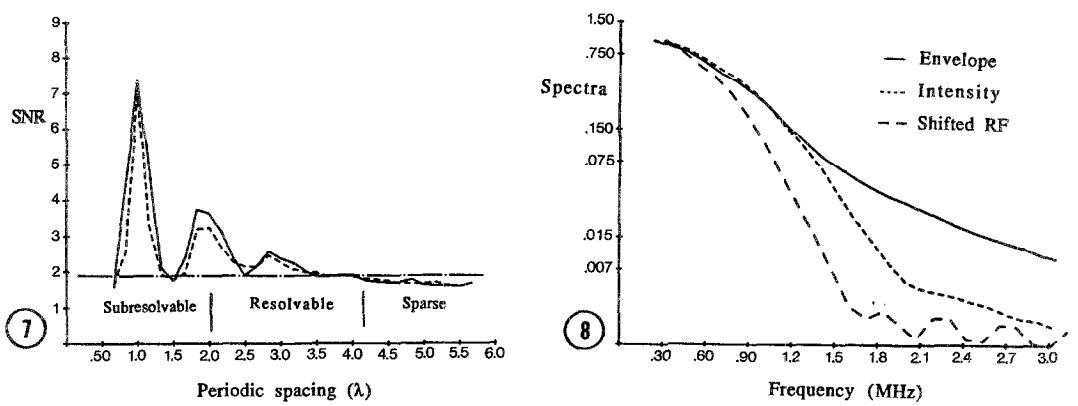

Fig. 7 Plot of SNR vs. periodic scatterer spacing. Dotted line shows effects from adding 10 percent amplitude and spacing jitter.

Fig. 8 Normalized spectra of envelope, intensity, and RF signal (center of spectrum shifted to 0) for dense random scatterers.

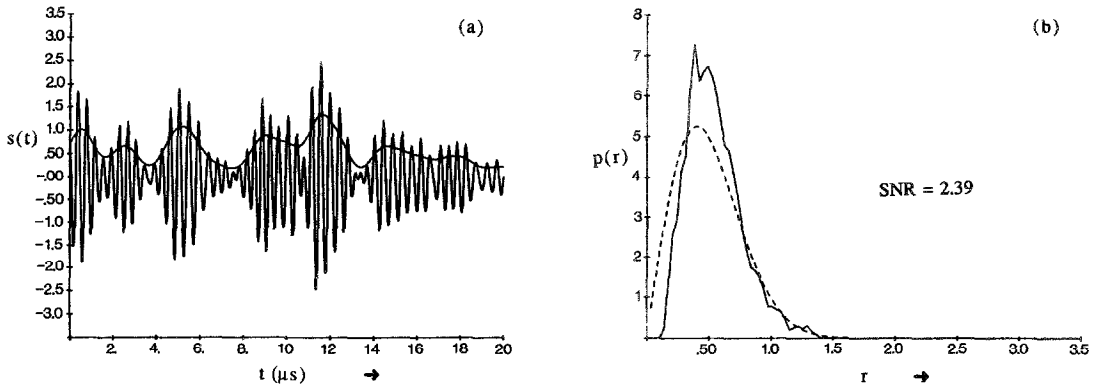

Fig. 9 a) Simulated RF signal for dense scatterers, and low pass filtered (1 MHz width) envelope. b) Corresponding envelope histogram with Rayleigh curve fit (dotted line).

IV. SYSTEM EFFECTS

a) Envelope Detection

In some clinical scanning devices and in some digital signal processing schemes, the ultrasound envelope is approximated by rectifying and low pass filtering the data. For a bandlimited RF signal, quadrature components will be bandlimited, and the intensity will also be bandlimited. However, the analytic envelope is not necessarily bandlimited [22]. This can be explained by the nonlinear step (positive square root in Eq. (2)) in processing, which generally results in the production of higher harmonics. Figure 8 shows the normalized amplitude spectra of a typical scan line, its intensity, and its envelope. The envelope is shown to have a wider bandwidth than the intensity. To examine the effects of filtering on the histograms, the dense scatterer RF signal was rectified and low-pass filtered with varying width Blackman filters. Using a 1 MHz lowpass filter, the envelope shows smoothed peaks and filled valleys (Fig. 9). The corresponding distribution appears shifted with a high SNR. As the filter bandwith is increased to 4 MHz, the envelope more closely outlines the RF signal (Fig. 10), and the distribution again approaches Rayleigh.

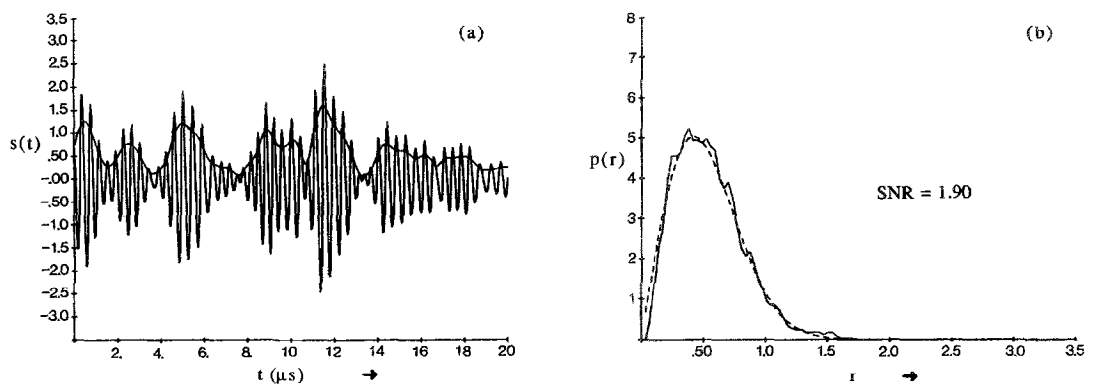

Fig. 10 a) Same RF signal as 9a, but envelope determined with 4 MHz low pass filter. b) Corresponding envelope histogram with Rayleigh curve fit (dotted line).

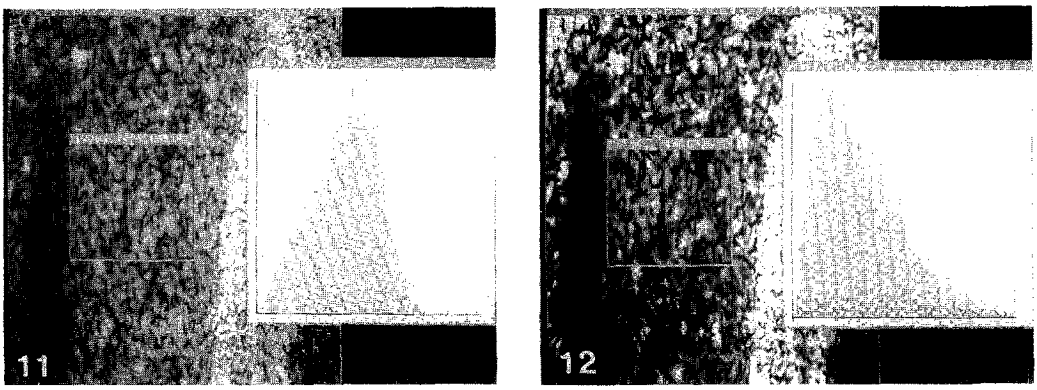

Fig. 11 Actual liver scan using Octoson with envelope histogram (inset) of blocked region. SNR = 2.71

Fig. 12 Decompressed image of figure 11 with envelope histogram (inset) of blocked region. SNR = 1.53

b) Log Amplification

Amplifier effects on the envelope distribution were also examined for actual clinical data. Using a liver scan obtained from the Octoson with 10 MHz sampling, a region was chosen with area comparable to that used in the simulations. The image shown in figure 11 is derived from RF signals which were log compressed for video display purposes. For this case the histogram displays a Rician-like distribution.

By decompressing the data (relinearizing using calibration data as outlined by Parker and Waag [23]), the histogram approaches Rayleigh, as shown in figure 12. The SNR is lower than 1.9 here due to the high amplitudes from the few strong specular scatterers included in the region of interest. This section of the liver would correspond to the bimodal model of figure 3, with fully developed speckle plus sparse, strong reflectors.

c) Other Effects

The simulations in section III are ideal cases in that the pulses are Gaussian and no attenuation or noise is present. To examine speckle statistics for more "realistic" scan lines, the RF signal was modified slightly. With the application of a wideband nonsymmetric pulse, the SNR decreased less than 10 percent for Rayleigh and periodic resolvable scatterers, and the subresolvable SNR peaks (as seen in figure 7) also decreased. The addition of 10 percent noise to the RF signals showed statistically insignificant differences for all cases. Attenuation, applied as an exponential along the scan lines, was also examined for periodic scatterers. For an attenuation coefficient of 0.125 np/cm, the approximate value for liver tissue at 2.5 MHz, the SNRs were reduced by about 5 to 20 percent for Rayleigh and resolvable scatterers and by up to 60 percent for subresolvable. Since most scanners have some gain compensation, a lower attenuation coefficient (0.035 np/cm) was also examined and shown to have negligible effects. Finally, changing the bandwidth of the Gaussian pulse did not affect the previous results as long as the number of scatterers per pulse width was consistent and the relation of the spacing with the wavelength was considered.

VI. CONCLUSIONS

This study shows that there are distinct requirements for generating both Rayleigh and Rician-like distributions. For Rayleigh statistics, at least five random scatterers per pulse width are needed. This limit is comparable to Oosterveld's results [20] if the sample volume is estimated from the reported transducer geometry. With the addition of regular scatterers, the distribution is highly dependent on amplitude, spacing as related to the wavelength, and jitter. Apparently, histograms which have a high SNR and resemble the Rician case can only be generated by having a densely packed random population in combination with regularly spaced, high amplitude reflectors with separations close to an integral number of wavelengths. More generally, the use of the SNR as a sole parameter appears insufficient and ambiguous for inferring scatterer population. However, the shape of the histogram may provide insight as to the class of scatterers or system effects which are influencing the signal.

A few guidelines are suggested for performing a statistical analysis. For tissue discrimination, a large region of interest is necessary in obtaining an averaged estimate of the SNR. For our simulations, which use an equivalent of 50 cm of independent scan lines, the SNRs of Rayleigh distributions ranged from 1.8 to 2.0. Care must also be taken when computing the envelope since it is non-bandlimited. If possible the analytic envelope should be calculated. Finally, any amplifier nonlinearities should be characterized and removed before proceeding with the analyses.

REFERENCES

[1] Burckhardt, C.B., Speckle in ultrasound B-mode scans, *IEEE Trans. Sonics and Ultrasonics SU-25*, 1-6 (1978).

[2] Abbott, J.G. and Thurstone, F.L., Acoustic speckle: theory and experimental analysis, *Ultrasonic Imaging 1*, 303-324 (1979).

[3] Goodman, J.W., Statistical Properties of Laser Speckle Patterns, in *Laser Speckle and Related Phenomena*, J. C. Dainty, ed., (Springer-Verlag, Berlin, 1975).

[4] Wells, P.N.T. and Halliwell, M., Speckle in ultrasonic imaging, *Ultrasonics 19*, 225-229 (1981).

[5] Bamber, J.C. and Daft, C., Adaptive filtering for reduction of speckle in ultrasonic pulse-echo images, *Ultrasonics 24*, 41-44 (1986).

[6] Bockus, H.L., *Gastroenterology*, (W.B. Saunders Co., Philadelphia, 1965).

[7] Shung, K.K. and Fei, D.Y., The Stochastic Nature of Echoes from Biological Tissues, in *IEEE Seventh Annual Conference of the Eng. in Med. and Biology Society*, pp. 241-243 (IEEE CH2198-0, 1985).

[8] Green, S.E., Joynt, L.F., Fitzgerald, P.J., Rubenson, D.S., and Popp, R.L., *In vivo* ultrasonic tissue characterization of human intracardiac masses, *Am. J. Cardiol. 51*, 231-236 (1983).

[9] Vieli, A., Heiserman, J., Schnittger, I., and Popp, R.L., An improved stochastic approach to RF amplitude analysis in ultrasonic cardiac tissue characterization, *Ultrasonic Imaging 6*, 139-151 (1984).

[10] Sommer, F.G., Joynt, L.F., Carroll, B.A., and Macovski, A., Ultrasonic characterization of abdominal tissue via digital analysis of backscattered waveforms, *Radiology 141*, 811-817 (1981).

[11] Sommer, F.G., Joynt, L.F., Hayes, D.L., and Macovski, A., Stochastic frequency-domain tissue characterization: application to human spleens *in vivo*, *Ultrasonics 20*, 82-86 (1982).

[12] Fellingham, L.L. and Sommer, F.G., Ultrasonic characterization of tissue structure in the *in vivo* human liver and spleen, *IEEE Trans. Sonics Ultrasonics SU-31*, 418-428 (1984).

[13] Wagner, R. F., Smith, S.W., Sandrik, J.M., and Lopez, H., Statistics of speckle in ultrasound B-scans, *IEEE Trans. Sonics Ultrasonics SU-30*, 156-163 (1981).

[14] Smith, S.W. and Wagner, R.F., Ultrasound speckle size and lesion signal to noise ratio: verification of theory, *Ultrasonic Imaging 6*, 174-180 (1984).

[15] Wagner, R.F., Insana, M.F., and Brown, D.G., Unified approach to the detection and classification of speckle texture in diagnostic ultrasound, *Optical Eng. 25*, 738-742 (1986).

[16] Insana, M. F., Wagner, R.F., Garra, B.S., Brown, D.G., and Shawker, T.H., Analysis of ultrasound image texture via generalized Rician statistics, *Optical Eng. 25*, 743-748 (1986).

[17] Wagner, R.F., Insana, M.F., and Brown, D.G., Statistical properties of radio-frequency and envelope-detected signals with applications to medical ultrasound, *J. Opt. Soc. Am. 4*, 910-922 (1987).

[18] Kuc, R., Ultrasonic tissue characterization using kurtosis, *IEEE Trans. Ultrason., Ferro., Freq. Control. UFFC-33*, 273-279 (1986).

[19] Middleton, D., *Statistical Communication Theory*, (McGraw-Hill, New York, 1960).

[20] Oosterveld, B.J., Thijssen, J.M., and Verhoef,W.A., Texture of B-mode echograms: 3-D simulations and experiments of the effects of diffraction and scatterer density, *Ultrasonic Imaging 7*, 142-160 (1985).

[21] Bickel, P.J. and Doksum, K.A., *Mathematical Statistics*, (Holden-Day, Oakland, 1977).

[22] Dugundji, J., Envelopes and pre-envelopes of real waveforms, *IRE Trans. Inform. Theory IT-4*, 53-57 (1958).

[23] Parker, K.J. and Waag, R.C., Measurement of ultrasonic attenuation within regions selected from B-scan images, *IEEE Trans. Biomed. Eng. BME-30*, 431-437 (1983).